Healing Tissues From the Inside Out: Infusible Biomaterial for Targeting and Treating Inflammatory Tissues via Intravascular Administration

Martin T. Spang, Ryan Middleton, Miranda Diaz, Raymond Wang, Jervaughn Hunter, Joshua Mesfin, Tori S. Lazerson, Saumya Bhatia, James Corbitt, Gavin D'Elia, Gerardo Sandoval-Gomez, Rebecca Kandell, Takayuki Kato, Sachiyo Igata, Colin Luo, Kent G. Osborn, Pedro Cabrales, Ester Kwon, Francisco Contijoch, Ryan R. Reeves, Anthony N. DeMaria, Karen L. Christman

University of California, San Diego

Abstract

Biomaterials, such as extracellular matrix (ECM) hydrogels, have been widely used in preclinical studies as injectable tissue engineering therapies; however, injectable therapies are limited as they can cause localized trauma or organ perforation. We have developed a new ECM therapy, the low molecular weight fraction derived from decellularized, digested ECM, for intravascular infusion. This new form of ECM can be infused after injury, specifically localize to injured tissues by coating the leaky microvasculature, and promote cell survival and tissue repair. In this study, we show the feasibility and targeting of intravascular ECM infusions using models of acute myocardial infarction (MI), traumatic brain injury, and pulmonary arterial hypertension. Furthermore, safety and efficacy were demonstrated in small and large animal models of acute MI following intracoronary infusion, which included using a clinically-relevant catheter in the large animal model. Functional improvements, specifically reduced left ventricular volumes and improved wall motion scores were observed after ECM infusions post-MI. Genes related to tissue repair and inflammation were differential expressed in response to ECM infusions. This study shows proof-of-concept for a new paradigm of delivering pro-healing ECM biomaterials via intravascular infusion to heal tissue from the inside out.

26

Extracellular matrices (ECM) derived from decellularized tissues have shown promising results as tissue engineering scaffolds as an acellular strategy for regenerative medicine[1-5]. In particular, decellularized ECM can be processed via enzymatic digestion into inducible hydrogels that can be injected for minimally-invasive delivery to tissues[6-9]. These degradable hydrogels are pro-survival, immunomodulatory, and promote neovascularization, among a host of other pro-regenerative functions[2,10-12].

Current decellularized ECM biomaterials are limited to surgically implanted patches or localized injections. We aimed to develop a new form of ECM that could be delivered via jntravascular infusion to target leaky vasculature, allowing for less invasive, more evenly distributed, and potentially earlier delivery since tissue access is not a concern. Acute delivery following injury could reduce cell death, promoting tissue salvage and maintenance. This delivery modality is not amenable to current ECM hydrogels because of their physical properties, which would not allow for passage into the gaps of leaky endothelium at the site of injury or disease.

RESULTS

Infusible ECM can be isolated and is capable of gelation

A myocardial ECM hydrogel was selected as a starting material (Fig. 1a-d) for its demonstrated efficacy in preclinical models[7-10,13] and translational proof-of-concept in a Phase I clinical trial[14]. While this material is injectable, it is a translucent suspension (Fig. 1d), which contains large submicron particulate, which would be too large to pass through leaky vasculature at sites of acute injury and/or inflammation[15,16].

To generate an intravascularly infusible ECM, an optimized centrifugation, dialysis, and sterile filtration protocol was developed to remove the high molecular weight peptides/proteins

(Fig. 1e). The supernatant was isolated from the high molecular weight pellet and dialyzed, yielding the low molecular weight fraction, infusible ECM (iECM), which could then be sterile filtered, lyophilized for long-term storage, and resuspended for injection/infusion (Fig. 1f). While the iECM did not gel at body temperature *in vitro* like the ECM hydrogel counterpart, it was still capable of gelation in tissue after subcutaneous injection (Fig. 1g). Scanning electron imaging of the gel demonstrated a nanofibrous architecture (Fig. 1h) similar to most ECM hydrogels[17].

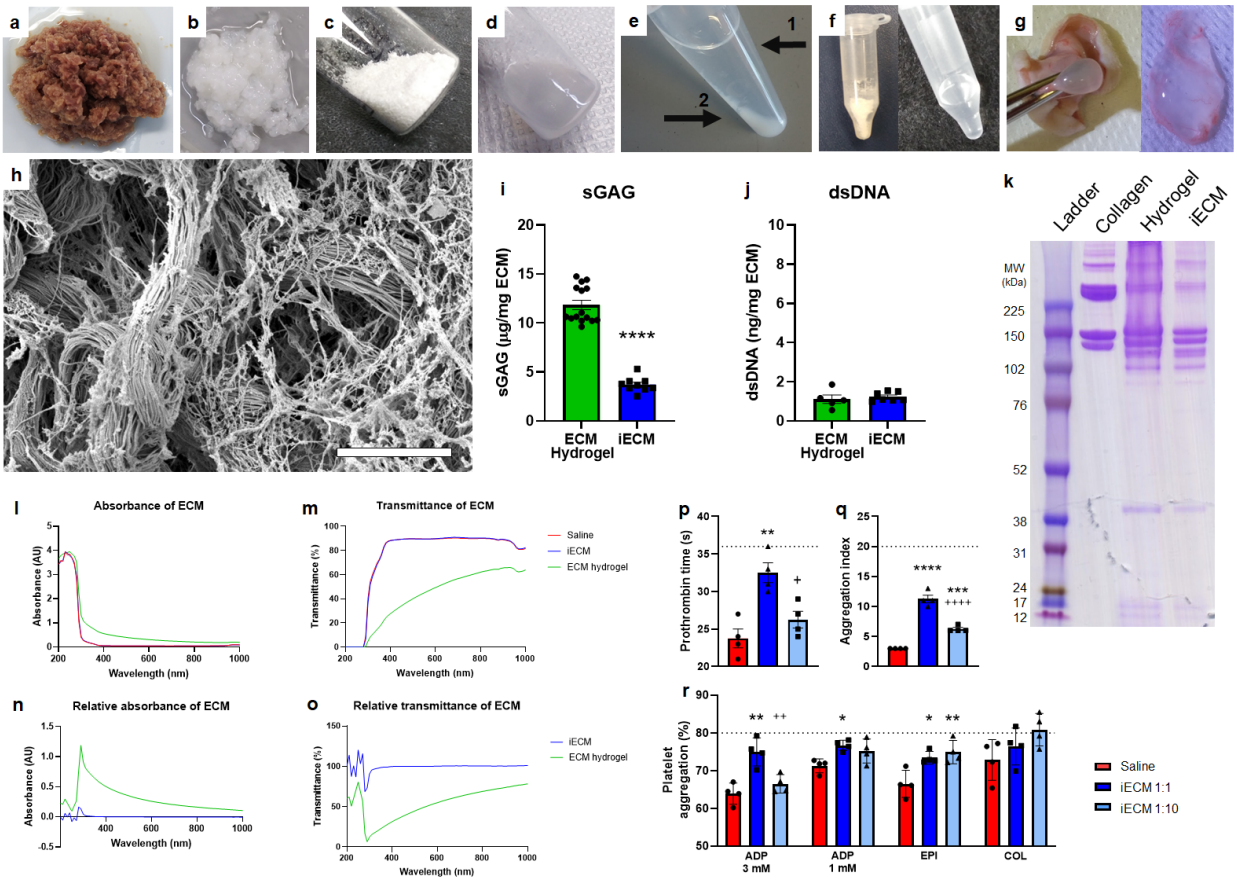

Figure 1: Generation and architecture of infusible extracellular matrix (iECM). **a**, Isolated left ventricular myocardium is cut into pieces. **b**, Decellularized ECM after continuous agitation in 1% sodium dodecyl sulfate. **c**, Lyophilized and milled ECM. **d**, Liquid digested ECM hydrogel. **e**, Fractionated ECM hydrogel after centrifugation; (1) supernatant low molecular weight fraction (iECM) and (2) high molecular weight pellet. **f**, Lyophilized (left) and resuspended (right) iECM.

g, Subcutaneous injection and gelation of iECM. **h**, Scanning electron microscopy image showing nanofibrous architecture of iECM following gelation. Scale bar is 5 μm. Characterization of iECM, **i**-**o**. **i**, Sulfated glycosaminoglycan (sGAG) content was significantly lower in iECM vs ECM hydrogel. **j**, Double stranded DNA (dsDNA) content was not significantly different between iECM and ECM hydrogel. **k**, Polyacrylamide gel electrophoresis of ladder (Full-Range RPN800E, lane 1), collagen (lane 2), ECM hydrogel (lane 3), and iECM (lane 4), showing depletion of high molecular weight (>200 kDa) peptides/proteins in iECM. **l**-**o**, Optical measurements of iECM vs liquid ECM hydrogel. iECM showed minimal differences in optical properties from saline whereas the ECM hydrogel possessed increased absorbance and decreased transmittance. **l**, Absorbance sweep of iECM, ECM hydrogel, and saline. **m**, Calculated transmittance of iECM, ECM hydrogel, and saline. **n**, Relative absorbance sweep of iECM and ECM hydrogel. **o**, Relative calculated transmittance of iECM and ECM hydrogel. Hemocompatibility of infusible extracellular matrix (iECM) with human blood and platelet rich plasma. **p**, Prothrombin time. **q**, Red blood cell aggregation index. **r**, platelet aggregation following addition of agonists: adenosine diphosphate (ADP), epinephrine (EPI), collagen (COL). Standard ranges for each parameter are indicated between or below dashed lines. * is relative to saline, and + is relative to iECM. Data are mean ± SEM. *$p<0.05$, **$p<0.01$, ***$p<0.001$, ****$p<0.0001$

When comparing iECM to the ECM hydrogel, sulfated glycosaminoglycan content was significantly decreased (Fig. 1i), whereas double stranded DNA content was not different (Fig. 1j). Gel electrophoresis showed a depletion of high molecular weight proteins (>200 kDa), which were likely removed during the fractionating process (Fig. 1k). Across most wavelengths tested, the optical properties of iECM were nearly identical to saline, whereas the liquid ECM hydrogel

87 showed increased absorbance and decreased transmittance (Fig. 1l-o), reinforcing the absence
88 of large particles in iECM.

89

90 **Infusible ECM is hemocompatible**

91 As iECM was derived from the ECM hydrogel, it was expected that iECM would be
92 hemocompatible. While it is counterintuitive to think that decellularized ECM could be
93 hemocompatible since exposed ECM initiates clotting *in vivo,* we previously demonstrated that
94 the ECM hydrogel was hemocompatible[9]. iECM was tested with human blood using the highest
95 likely scenario of 1:1 iECM to human blood and a physiologically relevant concentration of 1:10
96 iECM, given the immediate dilution with blood following infusion. Nearly all prothrombin times,
97 red blood cell aggregation indices, as well as platelet aggregation with agonists fall within
98 standard physiological ranges (Fig. 1p-r)[18,19]. Fibrinogen and platelet concentrations were
99 unaffected by the addition of iECM (Extended Data Fig. 1).

100

101 **ECM infusions target regions of injury in multiple preclinical models**

102 Three preclinical models were selected to cover diverse conditions in which leaky vasculature is
103 observed, specifically acute myocardial infarction (MI), traumatic brain injury (TBI), and
104 pulmonary arterial hypertension (PAH), which represent both acute and chronic injuries while
105 also covering ischemic, traumatic, and pressure overload injuries. iECM was delivered
106 intravascularly in all models with simulated intracoronary infusion in the MI model and
107 intravenous (IV) infusion in the TBI and PAH models. In the acute MI model (Fiz 2a-h), iECM
108 was localized to the infarcted region (Fig. 2a,b). Minimal material was observed in the border
109 zone (Fig. 2c), and no material was seen in the remote myocardium (Fig. 2d), including the
110 septum and right ventricle. In the TBI model (Fig. 2i-n), material was also localized to the region

of trauma (Fig. 2i,j) and no material was observed in remote brain (Fig. 2k). In the PAH model (Fig. 2o-s), material was localized throughout the lungs (Fig. 2o-p), as the PAH model affects the entire organ. All results observed histologically were also confirmed following near-infrared fluorescent scans (Fig. 2g,h, 2n, 2s). Biodistribution analysis suggested excess iECM accumulates in the liver and kidneys (Extended Data Fig. 2). As controls, saline or a small tagged non-gelling peptide (trilysine) control were infused and showed no retention (Fig. 2e,f, 2l, 2q, Extended Data Fig. 3), with the majority going to the kidneys (Extended Data Fig. 2).

Across all models, iECM was distributed specifically to injured tissues, suggesting leaky vasculature is required for material retention. To confirm this, iECM infusions were performed in healthy animals without MI (Extended Data Fig. 4), TBI (Fig. 2m), or PAH (Fig. 2r) as well in rats with a chronic MI, which does not have leaky vasculature (Extended Data Fig. 4). All of these animals showed minimal matrix retention in the target tissue; however, material was observed in the kidneys and urine, suggesting almost immediate elimination (Extended Data Fig. 4).

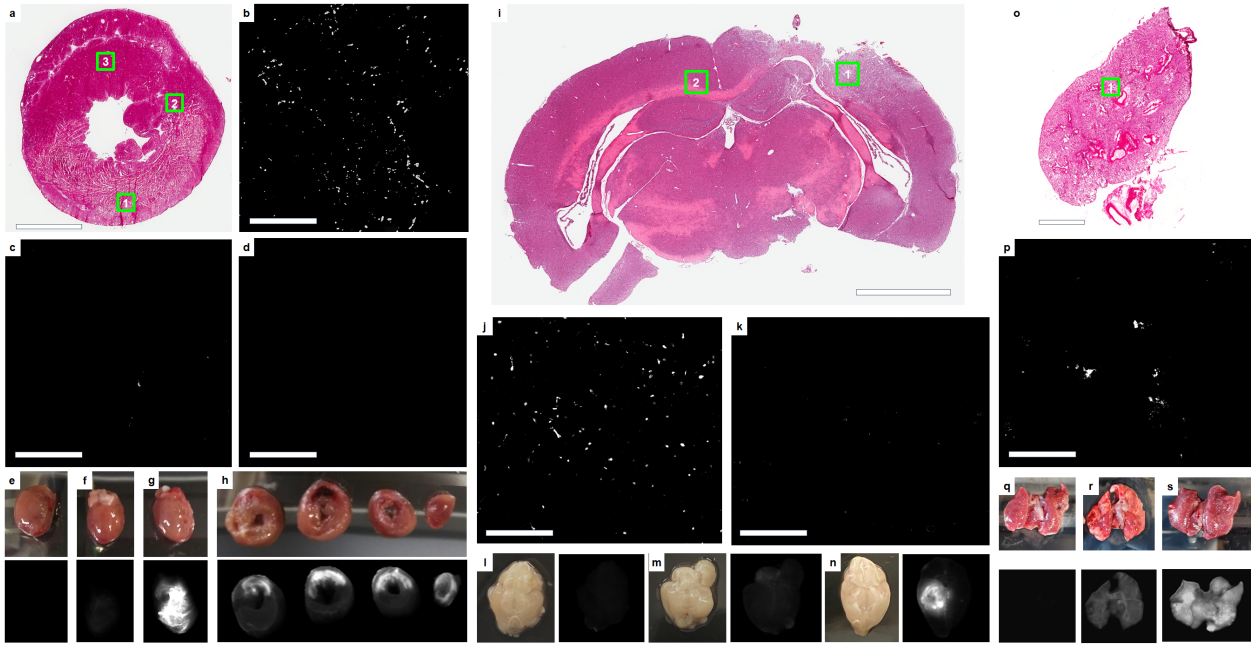

Figure 2: iECM infusions target injured tissues. **a**, H&E short axis section of an acute MI heart following iECM infusion, scale bar 3 mm. **b-d**, Fluorescence images for locations shown in insets in **a** of infarcted myocardium (**b**, 1), border zone (**c**, 2), and remote myocardium (**d**, 3), scale bars are 200 μm. **e-h**, Heart near-infrared scans of saline without dye (**e**), trilysine conjugated with VT750 (**f**), and iECM conjugated with VT750 (**g**). **h**, Short axis slices of an iECM infused heart from the base to the apex (left to right), infarct regions oriented in the upper portion of the slices. iECM tracking using VivoTag®-S 750 (VT750) 24 hours following infusion and MI procedure. **i,** H&E section of a brain following traumatic brain injury (TBI) and iECM infusion. **j-k**, Fluorescence images for locations shown in insets in **i** of injured brain (**j**, 1) or remote brain (**k**, 2). Near-infrared scans of brain infused with saline without dye following TBI (**l**), healthy brain infused with iECM conjugated with VT750 (**m**), and brain infused with iECM conjugated with VT750 following TBI (**n**). **o,** H&E section of a lung following monocrotaline injury, model of pulmonary arterial hypertension (PAH), and iECM infusion. **p**, Fluorescence image for location shown in inset in **o** of injured lung (1). Lung near-infrared scans of lung

143 infused saline without dye following PAH (**q**), healthy lung infused with iECM conjugated with
144 VT750 (**r**), and lung infused with iECM conjugated with VT750 following PAH (**s**).

145

146 Using the MI model, iECM showed a dose-dependent retention and distribution,
147 increasing from 6 to 10 mg/ml, but with no appreciable increase from 10 to 12 mg/ml (Extended
148 Data Fig. 5). However, due to manufacturing limitations, specifically filtration, 10 mg/ml was the
149 highest concentration that we could routinely produce. Furthermore, iECM was retained for
150 approximately 3 days following infusion (Extended Data Fig. 6).

151

152 **Infusible ECM shows co-localization with endothelial cells and reduces vascular leakage**

153 For safety evaluation, we wanted to confirm that iECM was not blocking the lumen of blood
154 vessels. We confirmed that iECM did not block arterioles (Fig. 3a), but we then observed that
155 the iECM aggregates were overlapping with the microvasculature network, specifically
156 endothelial cells (Fig. 3b). Upon further observation, confocal imaging suggested that material
157 was present within the gaps between endothelial cells, resembling a fibrous matrix, and/or
158 coating the inner lining, but not blocking the lumen of capillaries (Fig. 3c-g), leading to the
159 hypothesis that iECM infusions were reducing pathological tissue permeability by filling in the
160 gaps of leaky vasculature. In line with this hypothesis, iECM infusions significantly decreased
161 leakage of tagged BSA into the infarct (Fig. 4h-j), suggesting iECM reduced tissue permeability.
162 However, this did not affect neutrophil emigration (Extended Data Fig. 7).

163

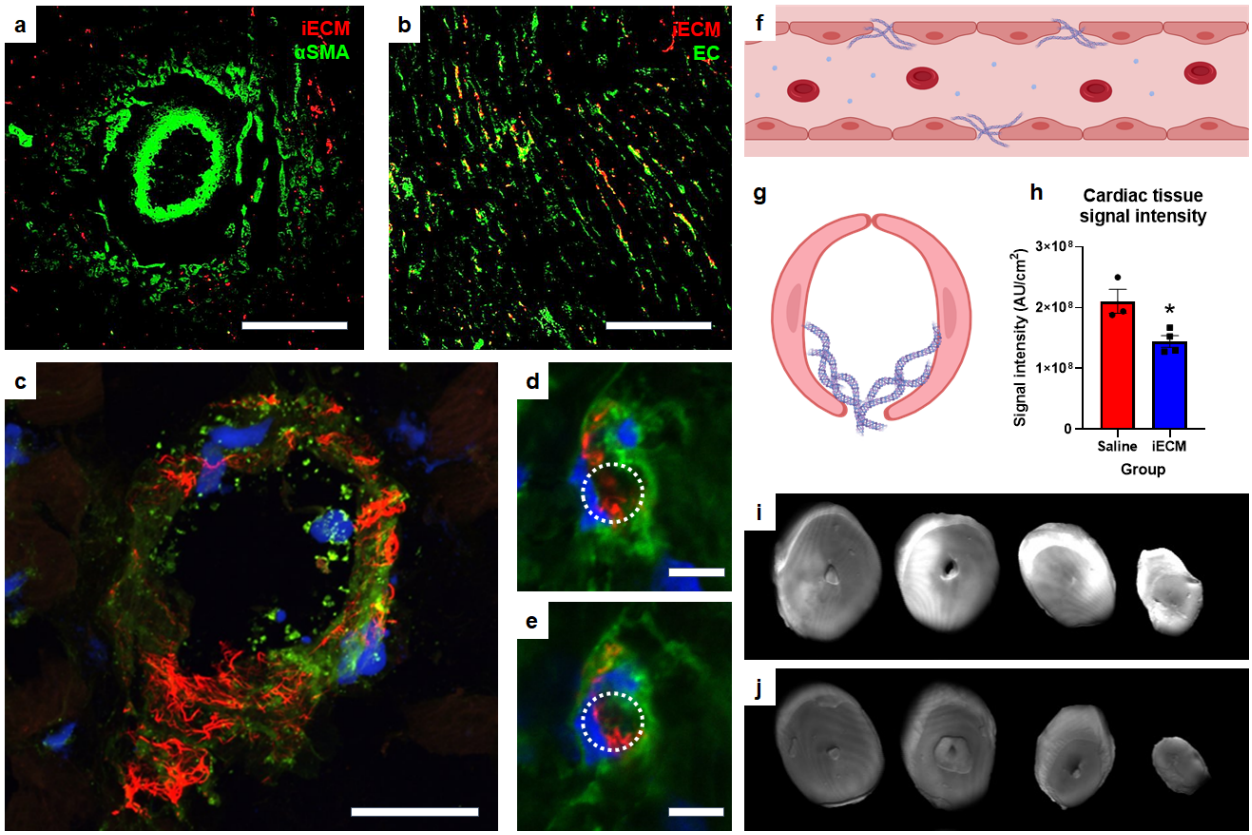

Figure 3: Staining for vasculature and iECM localization post-infusion and MI, showing colocalization of iECM with the microvasculature as opposed to large vessels. iECM was pre-labeled and visualized in red in all parts of Fig. 3. **a**, Staining for arterioles using anti-alpha smooth muscle actin (αSMA) in green. (**b**-**e**), Staining for endothelial cells using isolectin in green. Scale bar is 200 μm for **a**-**b**. **c**, iECM does not block the lumen of an arteriole but fills in the gaps in the endothelium. Scale bar is 25 μm. **d**,**e**, Representative sequential z-stack images of a capillary showing that iECM coats the lumen while not blocking it. Lumen traced with dotted white lines. Scale bar is 5 μm. **f**, Diagram of longitudinal axis view of iECM fibers coating a leaky vessel. **g**, Diagram of short axis view of iECM coating a capillary. **h**-**i,** Fluorescent scans of hearts following MI, intracoronary infusion (ICI) of saline (**h**) or iECM (**i**), and IV infusion of fluorescent bovine serum albumin (IV BSA). **j**, Quantified cardiac tissue signal intensity following

176 MI, ICI, and IV BSA, suggesting iECM infusions decrease tissue permeability. Data are mean ±
177 SEM. *p<0.05.

178

179 **Infusible ECM mitigates negative left ventricular remodeling in a rat acute MI model**

180 To test the efficacy of iECM in an acute MI model, rats were infused with iECM or saline
181 following occlusion-reperfusion (Fig. 4a-c). At 24 hours following infusions, iECM significantly
182 decreased LV volumes, both end-systolic (ESV, Fig. 4d) and diastolic volumes (EDV, Fig. 4e),
183 compared to the saline control alongside a trending increase in ejection fraction (EF, Fig. 4f).
184 We confirmed that this was not a result of differences in infarct size between groups (Extended
185 Data Fig. 8a-d) suggesting similar initial injuries. This significant decrease in LV volumes of
186 iECM animals was maintained at 5 weeks post-infusion as well.

187

188 **Infusible ECM is pro-survival and promotes tissue repair**

189 As ECM hydrogels have previously shown to promote tissue repair, including increases in
190 vascularization, being pro-survival, and modulation of inflammation[10,20], we hypothesized that
191 iECM would likewise have similar pro-reparative effects. At 5 weeks post-infusion, iECM
192 significantly increased infarct vascularization over controls (Fig. 4g-i). Infarct fibrosis and
193 interstitial fibrosis were not significantly different between groups (Supplemental Fig. 8e-g). At 3
194 days post-infusion (Fig. 4j), iECM significantly decreased the number of cardiomyocytes
195 undergoing apoptosis in the border zone region (Fig. 4k-m). We observed significant differential
196 expression of 11 and 23 genes at 1 day and 3 days post-infusion, respectively. Gene Ontology
197 (GO) pathway enrichment analysis suggested pathways, including angiogenesis, cell-substrate,
198 reactive oxygen species (ROS) and nitric oxide (NO) metabolism, and interleukin 6 (IL6) and
199 other cytokine signaling as illustrated by the Venn diagram of differentially expressed genes in

Figure 4n,o. The pathway distribution and full gene list are in Extended Data Tables 1 & 2. Heat maps of differentially expressed genes and the top 30 pathways from GO analysis can be viewed in Extended Data Figure 9 and Extended Data Tables 3 and 4, respectively.

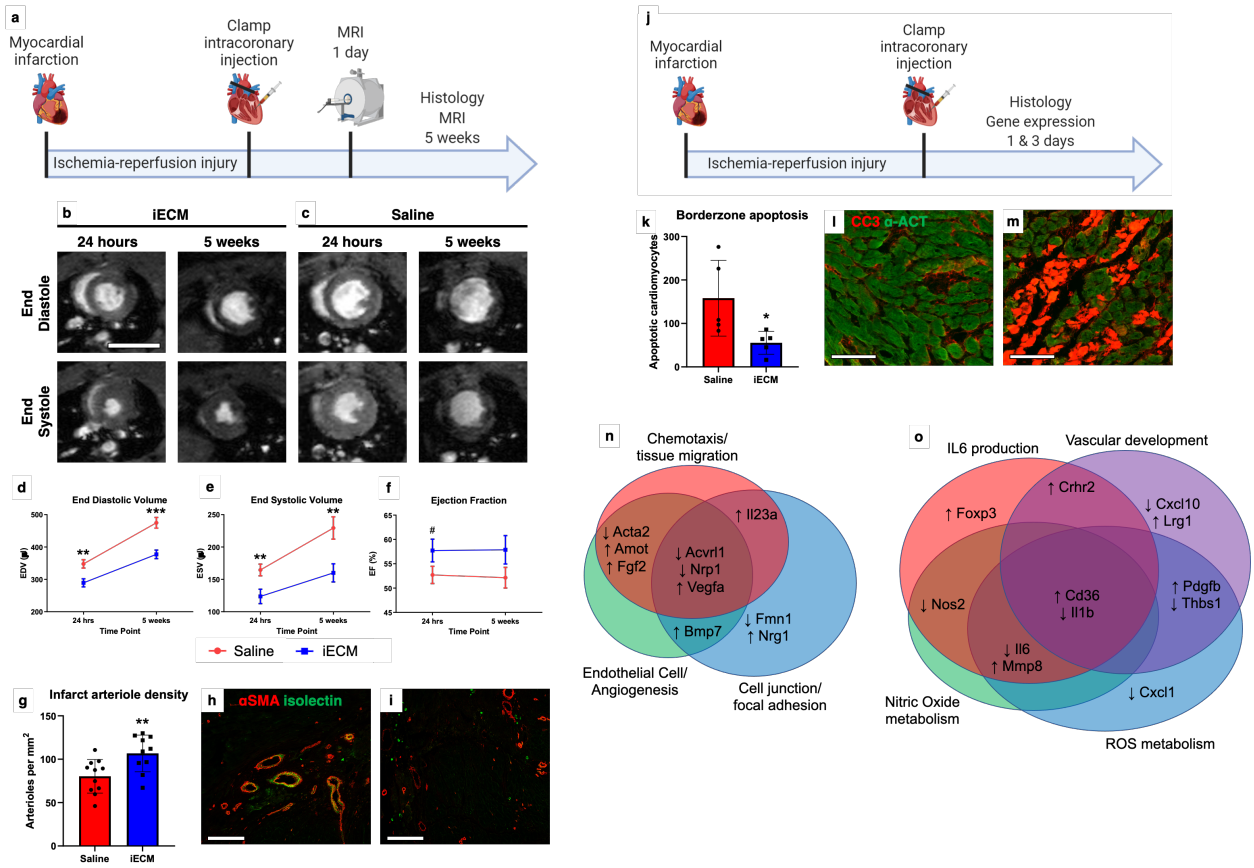

Figure 4: Infusible extracellular matrix (iECM) significantly improved cardiac function post-MI. **a**, Timeline of survival study. **b-c**, Representative magnetic resonance images at 24 hours and 5 weeks post-injection of iECM (**b**) or saline (**c**). Scale bar 10 mm. **d-f**, iECM infusions preserve left ventricle volumes at 24 hours and 5 weeks post-MI, end diastolic volume (**d**, EDV), end systolic volume (**e**, ESV), ejection fraction (**f**, EF). **g**, Infarct arteriole density increased with iECM infusions at 5 weeks post-infusion, promoting neovascularization. Representative images of iECM (**h**) and saline (**i**) infused hearts, alpha smooth muscle actin (αSMA) in red for arterioles and isolectin in green for endothelial cells. Scale bar 250 μm. **j**, Timeline of acute mechanisms

212 of repair study. Mechanisms of repair were evaluated through histology (**k**-**m**) and gene
213 expression (**n**-**o**) analyses. **k**, Number of cardiomyocytes undergoing apoptosis significantly
214 decreased in the border zone of iECM infused hearts at 3 days post-infusion. Representative
215 images of iECM (**l**) and saline (**m**) infused hearts, cleaved caspase 3 (CC3) for apoptosis in red,
216 and alpha actinin (α-ACT) for cardiomyocytes in green. Scale bar 100 μm. **n**-**o**, Gene
217 expression analysis from NanoString analysis at acute timepoints, suggesting genes related to
218 chemotaxis/tissue migration, endothelial cells/angiogenesis, and cell junction/focal adhesion
219 proteins are differentially expressed 1 day following iECM infusions and genes related to
220 Interleukin 6 (IL6), vascular development, nitric oxide metabolism, and reactive oxygen species
221 (ROS) metabolism are differentially expressed at 3 days following infusion. Data are mean ±
222 SEM.*$p<0.05$, **$p<0.01$, ***$p<0.001$, $^{\#}p<0.10$.

223

224 **Infusible ECM is amenable to intracoronary infusion with a clinically-relevant catheter**

225 Given the promising results in the small animal acute MI model, we tested if iECM could also be
226 delivered using a clinically-relevant infusion catheter in a large animal model. To ensure that
227 iECM would pass through a catheter, pre-gel complex viscosity was measured (Fig. 5a). The
228 pre-gel complex viscosity of iECM was an order of magnitude lower than the liquid ECM
229 hydrogel, but still higher than saline (Fig. 5a). Despite the increased viscosity, iECM was able to
230 pass through a catheter with an internal diameter of 0.36 mm. To assess clinical feasibility, a
231 balloon infusion catheter was used to induce MI and infuse tagged iECM (Fig. 5b). As seen in
232 the small animal model, iECM was observed in the infarct region in the porcine MI model (Fig
233 5c,d). Likewise, iECM was distributed throughout the infarcted myocardium and was not
234 observed in the border zone or remote myocardium (Extended Data Fig. 10). Satellite organs
235 did not show any signs of material, or acute ischemia or inflammation (Extended Data Fig. 11,
236 Extended Data Table 5). iECM was observed to similarly line endothelial cells of the infarcted

237 myocardium in the pig model (Fig. 5e,f). No signal was observed in the infarct region with a
238 small peptide control (Extended Data Fig. 10).

239

240 **Infusible ECM mitigates negative left ventricular remodeling in a porcine acute MI model**

241 To optimize material retention, volumes ranging from 1 ml to 10 ml were infused following MI,
242 demonstrating a plateau effect at 4 ml, suggesting that any additional infused iECM would not
243 be retained, as the microvasculature may be saturated (Fig. 5g). Subsequently, pigs underwent
244 MI, iECM or saline infusion, and serial echocardiography (echo) (Fig. 5h-x, Extended Data Fig.
245 12). Immediately post-MI, EDV, ESV, EF, and infarct angle, a measure of infarct area (Extended
246 Data Fig. 12h), were not significantly different between groups, suggesting a similar injury
247 between groups. EDV, ESV, and EF were measured over time (Fig. 5i,k,m) showing iECM
248 significantly reduced the expansion in EDV from immediately post-MI to 8 weeks later compared
249 to saline (Fig. 5j,o) with a similar trending improvement in the change in ESV (5l) and significant
250 improvement in the change in LV systolic dimension from post-MI to 8 weeks post-MI (Extended
251 Data Fig. 12e). While the change in EF was not significantly different (Fig. 5n), there was
252 significant improvement in the change in fractional shortening (Extended Data Fig. 12g).

253 Shortly post-MI and iECM infusion, LV wall thickness was significantly decreased (Fig.
254 5p,q), while infarct angle was significantly reduced at 7 days and 8 weeks post-MI (Fig. 5r)
255 compared to saline. Global wall motion index scores also showed similar improvements (Fig.
256 5s) with significant differences in the change from post-MI to 7 days (Fig. 5t) and 8 weeks (Fig.
257 5u). This was attributed to significant improvements in infarcted wall segments (B, C, K, and L)
258 over time, whereas no improvements were observed for saline infused hearts (Fig. 5v-x). ECG
259 and Holter monitoring analysis showed no differences in arrythmias between groups.

260

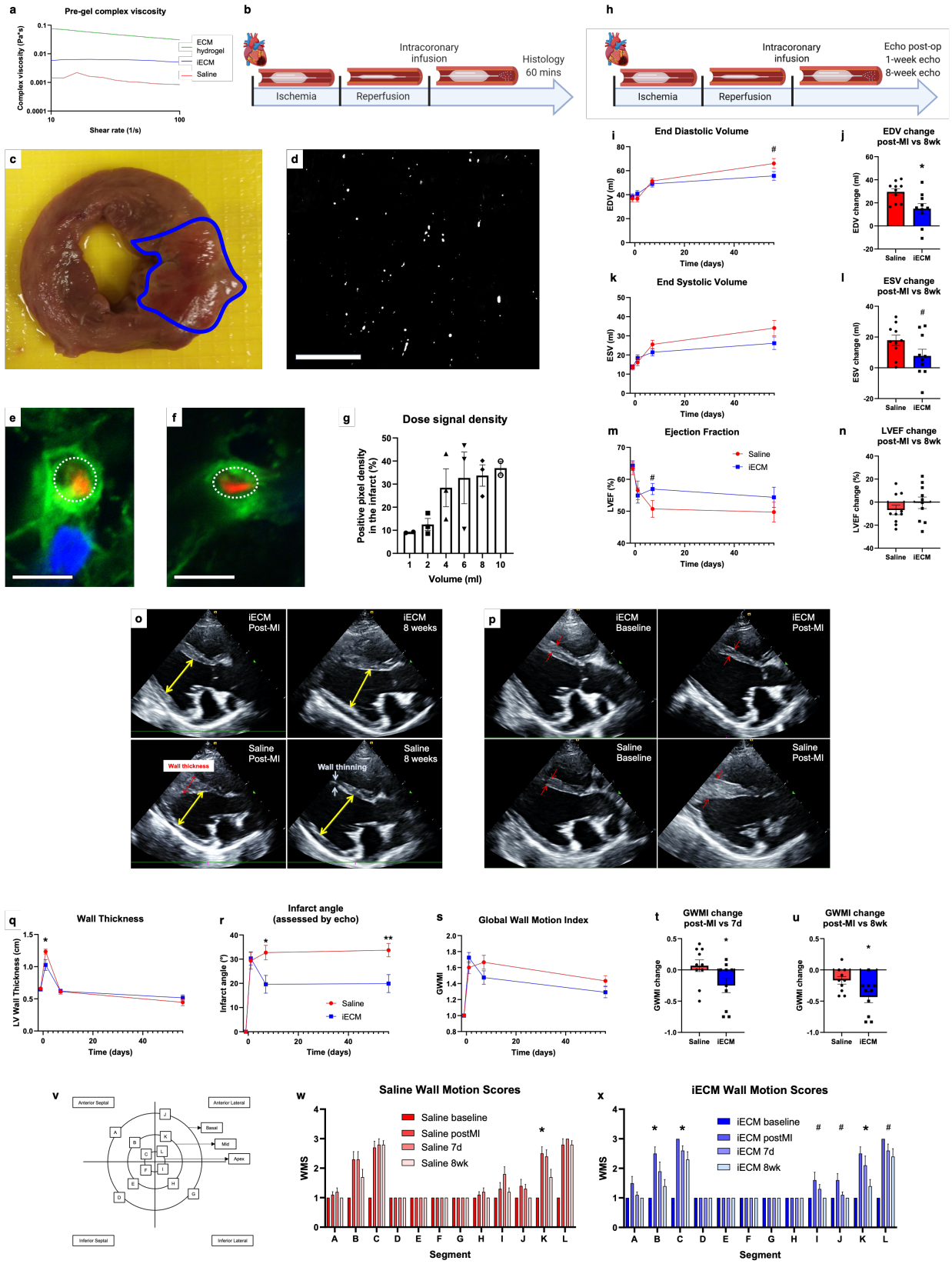
a
Pre-gel complex viscosity
Complex viscosity (Pa*s)
Shear rate (1/s)
ECM hydrogel
iECM
Saline
b
Ischemia
Reperfusion
Intracoronary infusion
Histology 60 mins
h
Ischemia
Reperfusion
Intracoronary infusion
Echo post-op
1-week echo
8-week echo
c
d
e
f
g
Dose signal density
Positive pixel density in the infarct (%)
Volume (ml)
i
End Diastolic Volume
EDV (ml)
Time (days)
j
EDV change post-MI vs 8wk
EDV change (ml)
Saline
iECM
k
End Systolic Volume
ESV (ml)
Time (days)
l
ESV change post-MI vs 8wk
ESV change (ml)
m
Ejection Fraction
LVEF (%)
Time (days)
Saline
iECM
n
LVEF change post-MI vs 8wk
LVEF change (%)
o
iECM Post-MI
iECM 8 weeks
Saline Post-MI
Wall thickness
Saline 8 weeks
Wall thinning
p
iECM Baseline
iECM Post-MI
Saline Baseline
Saline Post-MI
q
Wall Thickness
LV Wall Thickness (cm)
Time (days)
r
Infarct angle (assessed by echo)
Infarct angle (°)
Time (days)
Saline
iECM
s
Global Wall Motion Index
GWMI
Time (days)
t
GWMI change post-MI vs 7d
GWMI change
Saline
iECM
u
GWMI change post-MI vs 8wk
GWMI change
Saline
iECM
v
Anterior Septal
Anterior Lateral
Basal
Mid
Apex
Inferior Septal
Inferior Lateral
w
Saline Wall Motion Scores
Saline baseline
Saline postMI
Saline 7d
Saline 8wk
WMS
Segment
x
iECM Wall Motion Scores
iECM baseline
iECM postMI
iECM 7d
iECM 8wk
WMS
Segment

261

262 Figure 5: iECM infusions are amenable to intracoronary infusion with a balloon infusion catheter
263 and mitigate negative left ventricular remodeling in a pig acute MI model. **a**, iECM pre-gel
264 complex viscosity is lower than its full ECM hydrogel counterpart, suggesting potential for
265 catheter delivery. **b**, Timeline of catheter feasibility study. **c**, Macroscopic short-axis view of a
266 pig heart post-MI and iECM infusion. Infarct outlined in blue. **d**, Fluorescent image of iECM
267 distribution and retention in a histological section from the same heart. Scale bar 200 μm. **e**,**f**,
268 Representative confocal images of iECM (red) and endothelial cells (green) from iECM infused
269 pigs. iECM lines the endothelial cells of infarcted myocardium, as similarly observed in the rat
270 MI model. Lumen traced with dotted white lines; Scale bars 5 μm. **g**, iECM infusions showed a
271 plateau effect when increasing infusion volumes, as suggested by quantified signal density in
272 the infarct. **h**, Timeline of survival study following induced MI and iECM or saline infusion. End
273 diastolic volume (EDV), end systolic volume (ESV), ejection fraction (EF), left ventricular (LV)
274 wall thickness, infarct angle, global wall motion index (GWMI), and wall motion scores (WMS)
275 were measured before MI (baseline), post-MI, 7 days, and 8 weeks post-MI. **h-u**, Changes in
276 EDV, ESV, and EF over time (**i,k,m**) and relative to post-MI (**j,l,n**), suggest iECM infusions
277 mitigate negative left ventricular remodeling. Representatives echocardiography images at end
278 diastole show how iECM infusions mitigate negative LV remodeling from post-MI to 8 weeks
279 post-MI (**o**) and mitigate acute increases in wall thickness post-MI (**p**). Red arrows indicate wall
280 thickness, yellow arrows are used for LV end diastolic measurement. Changes in MI wall
281 thickness (**q**), infarct angle (**r**), GWMI (**s-u**), and WMS segments (**v-x**) over time, showing how
282 iECM infusions preserve LV wall thickness and motion and mitigate infarct expansion. Wall
283 motion score diagram used for scoring wall motion (**v**). Data are mean ± SEM. *$p<0.05$, $^{\#}p<0.10$.

284
285
286
287

288 **Discussion**

289 In this study, we developed a new form of decellularized ECM for intravascular infusion
290 as a new acellular strategy for regenerative medicine. We demonstrated feasibility of delivering
291 iECM intravascularly to target injured and diseased tissue with leaky vasculature, showing
292 broad applicability in acute MI, TBI, and PAH models. iECM was hemocompatible and we found
293 no evidence of embolization, demonstrating the material can be safely delivered intravascularly.
294 Furthermore, in small and large animal acute MI models, therapeutic efficacy was observed,
295 indicating the potential for clinical translation. The material was only observed in injured tissues
296 with leaky vasculature, demonstrating that iECM retention and therapeutic efficacy is conserved
297 across species and injury models.

298 Our initial hypothesis was that iECM would pass through the gaps in the endothelial cell
299 layer in the leaky vasculature and into the injured tissue as was previously seen with an
300 infusible alginate material[21]. Instead, we found that iECM coats and/or fills in the gaps between
301 endothelial cells (Fig. 3), specifically in regions of damaged tissues, and therefore represents a
302 new type of targeted delivery for pro-healing biomaterials. This localization led to a reduction in
303 vascular permeability (Fig. 3h-j), with potential reduction in tissue edema, which, in the case of
304 MI, is known to contribute to cardiac cell dysfunction and death[22,23]. As observed in the pig MI
305 model, wall thickness was significantly reduced post-MI, suggesting a barrier to fluid and/or
306 small proteins. As myocardial edema begins during ischemia and quickly expands following
307 reperfusion[24], acute iECM infusions could prevent tissue edema and further tissue damage from
308 reperfusion injury. Tissue edema is also observed in numerous pathologies with leaky
309 vasculature, including TBI[25,26] and PAH[27,28], suggesting iECM could be a novel therapeutic
310 approach for such conditions.

311 To demonstrate the therapeutic of potential of iECM we extensively tested it in both
312 small and large animal MI models, including the use of clinically relevant catheter procedures in

313 the latter. iECM significantly reduced both end-diastolic and end-systolic volumes one day after
314 MI and infusion in rats. This difference was maintained, but did not further improve out to 5
315 weeks post-infusion (Fig 4d,e), essentially creating a better baseline. This is in line with the
316 observed degradation time of iECM, approximately 3 days, where there is an initial therapeutic
317 effect. Therapeutic efficacy was also observed in the porcine model where iECM mitigated an
318 increase in EDV from post-MI to 8 weeks post-MI, reinforcing that iECM infusions reduce
319 negative LV remodeling. Significant improvements in infarct angle and wall motion were also
320 observed in the porcine model, further suggesting localized therapeutic efficacy and
321 improvements in regional function.

322 In terms of biological activity, ECM hydrogels have been shown to create a pro-
323 remodeling versus a pro-inflammatory environment, leading to increases in vascularization and
324 cell survival[7,10,31]. We found decreased numbers of apoptotic cardiomyocytes and increased
325 arteriole density with the iECM infused rat hearts. However, based on the finding that iECM
326 coats endothelial cells as opposed to entering the tissue, the mechanisms leading to improved
327 survival and vascularization are likely different between the iECM and ECM hydrogels. From
328 gene expression analyses, angiogenic, endothelial cells, and cell migration/recruitment
329 pathways were expected and dominated the pathway analysis 1 day following iECM infusions. It
330 was unexpected to see several pathways around focal adhesions and cell-substrate junctions.
331 The focal adhesion and cell-substrate pathways may suggest how the treated endothelial cells
332 adapt in response to iECM infusions, as endothelial cells would be directly exposed immediately
333 post-infusion. At 3 days post-infusion, ROS and NO metabolism and IL6 signaling emerged. It is
334 possible that iECM infusions encourage healthy ROS metabolism or the iECM itself provides an
335 ROS sink and/or protection for the surrounding cells as has been shown with the ECM
336 hydrogel[32], leading to decreased apoptosis. IL6 downregulation at 3 days post-MI would

337 suggest that iECM infusions encourage this pro-regenerative switch to happen earlier, reducing
338 negative LV remodeling[33].

339 Even though iECM is derived from an ECM hydrogel, it could be more appropriate to
340 compare iECM to peptide therapeutics given its delivery modality. This comparison to peptides
341 is evident in the clearance of non-retained iECM, which like other peptide therapeutics[29,30]
342 appears to be rapidly excreted by the kidneys (Extended Data Fig. 2). However, iECM has
343 advantages over traditional peptide therapeutics due to increased retention through potential
344 binding and gelation in the gaps of leaky vasculature (Fig. 3c). This could shield the material
345 from proteolysis, allowing for increased tissue retention and therapeutic effects over peptides
346 therapeutics[30].

347 ECM infusions are a versatile new platform for the regenerative medicine and tissue
348 engineering field. In this study, we chose to focus on the cardiac application of ECM infusions;
349 however, infusible ECM could be generated from any type of decellularized tissue, and ECM
350 infusions could be applied to many diseases or injuries where there is endothelial cell injury or
351 dysfunction. Whereas traditional tissue engineering approaches have focused on scaffolds
352 and/or cells to replace or repair damaged tissue, infusible ECM therapies could shift the focus
353 towards treating the microvasculature and healing tissues from the inside out to improve tissue
354 function.

Acknowledgements

Funding was provided by the NIH NHLBI (R01HL113468, R43HL150917). MTS was supported by NIH NHLBI T32HL105373 and an AHA pre-doctoral fellowship. The authors would like to thank Jesse Placone for his confocal imaging assistance, Pamela Duran for her helpful comments during the manuscript editing process, and the University of California, San Diego Institutional Animal Care and Use Program veterinary staff for their assistance with large animal procedures and safety. Schematic figures were created with BioRender.com.

Author contributions

KLC obtained the funding. MTS, KLC, RRR, and AND conceptually designed the studies. MTS, KLC, and AND interpreted the results. CL performed small animal surgeries. SI performed large animal echocardiography. RRR performed large animal surgeries. KGO performed large animal necropsy and histopathology analysis. MTS, RM, MD, RW, JH, JM, TSL, SB, JC, RK, and GS processed tissue samples and performed analyses. RM, RW, JH, JM, TK, and CL assisted with large animal surgeries. MD and RW assisted with gene expression analyses. PC designed and performed hemocompatibility analysis. EK and FC provided consultation, experimental design, and data evaluation related to imaging. MTS and KLC drafted the manuscript. All authors edited the manuscript.

Competing interests

KLC and AND hold equity in Ventrix, Inc. KLC is a co-founder, consultant, and board member of Ventrix, Inc.

Additional information

Supplementary information is available for this paper online.

Correspondence and requests for materials should be addressed to KLC.

References

1. Badylak, S.F. The extracellular matrix as a biologic scaffold material. *Biomaterials* **28**, 3587-3593 (2007).
2. Saldin, L.T., Cramer, M.C., Velankar, S.S., White, L.J. & Badylak, S.F. Extracellular matrix hydrogels from decellularized tissues: Structure and function. *Acta Biomaterialia* **49**, 1-15 (2017).
3. Spang, M.T. & Christman, K.L. Extracellular matrix hydrogel therapies: In vivo applications and development. *Acta Biomaterialia* **68**, 1-14 (2018).
4. Badylak, S.F., Freytes, D.O. & Gilbert, T.W. Extracellular matrix as a biological scaffold material: Structure and function. Vol. 5 1-13 (2009).
5. Christman, K.L. Biomaterials for tissue repair. *Science* **363**, 340-341 (2019).
6. Freytes, D.O., Martin, J., Velankar, S.S., Lee, A.S. & Badylak, S.F. Preparation and rheological characterization of a gel form of the porcine urinary bladder matrix. *Biomaterials* **29**, 1630-1637 (2008).
7. Singelyn, J.M.*, et al.* Naturally derived myocardial matrix as an injectable scaffold for cardiac tissue engineering. *Biomaterials* **30**, 5409-5416 (2009).
8. Singelyn, J.M.*, et al.* Catheter-deliverable hydrogel derived from decellularized ventricular extracellular matrix increases endogenous cardiomyocytes and preserves cardiac function post-myocardial infarction. *Journal of the American College of Cardiology* **59**, 751-763 (2012).
9. Seif-Naraghi, S.B.*, et al.* Safety and efficacy of an injectable extracellular matrix hydrogel for treating myocardial infarction. *Science translational medicine* **5**, 173ra125-173ra125 (2013).
10. Wassenaar, J.W.*, et al.* Evidence for Mechanisms Underlying the Functional Benefits of a Myocardial Matrix Hydrogel for Post-MI Treatment. *Journal of the American College of Cardiology* **67**, 1074-1086 (2016).
11. Dziki, J.L. & Badylak, S.F. Immunomodulatory Biomaterials. *Current Opinion in Biomedical Engineering* (2018).
12. Sadtler, K.*, et al.* Proteomic composition and immunomodulatory properties of urinary bladder matrix scaffolds in homeostasis and injury. *Seminars in Immunology* **29**, 14-23 (2017).
13. Wang, R.M. & Christman, K.L. Decellularized myocardial matrix hydrogels: In basic research and preclinical studies. *Advanced Drug Delivery Reviews* **96**, 77-82 (2016).
14. Traverse, J.H.*, et al.* First-in-Man Study of a Cardiac Extracellular Matrix Hydrogel in Early and Late Myocardial Infarction Patients. *JACC: Basic to Translational Science* (2019).
15. Hobbs, S.K.*, et al.* Regulation of transport pathways in tumor vessels: Role of tumor type and microenvironment. *Proceedings of the National Academy of Sciences of the United States of America* **95**, 4607-4612 (1998).
16. Alexis, F., Pridgen, E., Molnar, L.K. & Farokhzad, O.C. Factors affecting the clearance and biodistribution of polymeric nanoparticles. Vol. 5 505-515.
17. Ungerleider, J.L., Johnson, T.D., Rao, N. & Christman, K.L. Fabrication and characterization of injectable hydrogels derived from decellularized skeletal and cardiac muscle. *Methods (San Diego, Calif.)* **84**, 53-59 (2015).
18. White, M.M. & Jennings, L.K. *Platelet Protocols: Research and Clinical Laboratory Procedures*, (1999).
19. Vayá, A.*, et al.* Erythrocyte aggregation determined with the Myrenne aggregometer at two modes (M0, M1) and at two times (5 and 10 sec). Vol. 29 119-127 (2003).
20. Gaetani, R.*, et al.* Cardiac-Derived Extracellular Matrix Enhances Cardiogenic Properties of Human Cardiac Progenitor Cells. *Cell Transplantation* **25**, 1653-1663 (2016).

21. Leor, J.*, et al.* Intracoronary Injection of In Situ Forming Alginate Hydrogel Reverses Left Ventricular Remodeling After Myocardial Infarction in Swine. *Journal of the American College of Cardiology* **54**, 1014-1023 (2009).
22. Garcia-Dorado, D., Andres-Villarreal, M., Ruiz-Meana, M., Inserte, J. & Barba, I. Myocardial edema: A translational view. Vol. 52 931-939 (Elsevier, 2012).
23. Dongaonkar, R.M., Stewart, R.H., Geissler, H.J. & Laine, G.A. Myocardial microvascular permeability, interstitial oedema, and compromised cardiac function. Vol. 87 331-339 (Oxford University Press, 2010).
24. Thuny, F.*, et al.* Post-conditioning reduces infarct size and edema in patients with ST-segment elevation myocardial infarction. *Journal of the American College of Cardiology* **59**, 2175-2181 (2012).
25. Habgood, M.D.*, et al.* Changes in blood-brain barrier permeability to large and small molecules following traumatic brain injury in mice. *European Journal of Neuroscience* **25**, 231-238 (2007).
26. Higashida, T.*, et al.* The role of hypoxia-inducible factor-1α, aquaporin-4, and matrix metalloproteinase-9 in blood-brain barrier disruption and brain edema after traumatic brain injury: Laboratory investigation. *Journal of Neurosurgery* **114**, 92-101 (2011).
27. Zhou, C., Townsley, M.I., Alexeyev, M., Voelkel, N.F. & Stevens, T. Endothelial hyperpermeability in severe pulmonary arterial hypertension: Role of store-operated calcium entry. *American Journal of Physiology - Lung Cellular and Molecular Physiology* **311**, L560-L569 (2016).
28. Sugita, T.*, et al.* Lung vessel leak precedes right ventricular hypertrophy in monocrotaline-treated rats. *Journal of Applied Physiology Respiratory Environmental and Exercise Physiology* **54**, 371-374 (1983).
29. Fosgerau, K. & Hoffmann, T. Peptide therapeutics: current status and future directions. *Drug Discovery Today* **20**(2015).
30. Di, L. Strategic Approaches to Optimizing Peptide ADME Properties. *AAPS Journal* **17**, 134-143 (2015).
31. Ungerleider, J.L.*, et al.* Extracellular Matrix Hydrogel Promotes Tissue Remodeling, Arteriogenesis, and Perfusion in a Rat Hindlimb Ischemia Model. *JACC: Basic to Translational Science* **1**(2016).
32. Wang, R.M.*, et al.* Myocardial matrix material supports a proliferative microenvironment for cardiomyocytes. *bioRxiv*, 2020.2007.2031.231845-232020.231807.231831.231845 (2020).
33. Fontes, J.A., Rose, N.R. & Čiháková, D. The varying faces of IL-6: From cardiac protection to cardiac failure. Vol. 74 62-68 (Academic Press, 2015).